Published in final edited form as:
Nano Lett. 2011 July 13; 11(7): 2809–2813. doi:10.1021/nl201166k.

Controlled Growth of Nanoparticles from Solution with *In Situ* Liquid Transmission Electron Microscopy

James E. Evans[1,3,*], **Katherine L. Jungjohann**[2], **Nigel D. Browning**[1,2,3], and **Ilke Arslan**[2]

[1] Department of Molecular and Cellular Biology, University of California, Davis, Davis, CA 95616

[2] Department of Chemical Engineering and Materials Science, University of California, Davis, Davis, CA 95616

[3] Physical Life Sciences Directorate, Lawrence Livermore National Laboratory, Livermore, CA 94550

Abstract

Direct visualization of lead sulfide nanoparticle growth is demonstrated by selectively decomposing a chemical precursor from a multi-component solution using *in situ* liquid transmission electron microscopy. We demonstrate reproducible control over growth mechanisms that dictate the final morphology of nanostructures while observing growth in real-time with sub-nanometer spatial resolution. Furthermore, while an intense electron beam can initiate nanoparticle growth, it is also shown that a laser can trigger the reaction independently of the imaging electrons.

Keywords

In situ TEM; liquid TEM; fluid TEM; nanoparticle growth; Dynamic TEM; DTEM

Precise and reproducible control of the size and shape of 0-, 1- and 2-dimensional nanomaterials is a central goal of nanotechnology [1]. The recent development of *in situ* liquid transmission electron microscopy (TEM) has advanced our understanding of nanostructure dynamics. This method was pioneered for battery research focused on visualizing copper deposition on gold electrodes [2, 3]. Since that time, similar stages have been used for biological research imaging chemically-fixed whole cells labeled with gold nanoparticles selective for specific proteins of interest [4–6], and nanotechnology research investigating colloidal interactions in aqueous liquid [7, 8]. Previous results highlighting nanoparticle growth with *in situ* liquid TEM employed the reduction of Pt(acetylacetonate)$_2$ via intense parallel electron beam illumination to form colloidal platinum nanoparticles within a sealed environmental chamber [7]. However, for any reaction to take place within a sealed environmental chamber all required chemicals must be present in solution prior to insertion within the microscope, which can be an issue for multi-component and multi-stage reactions. Another limitation to sealed environmental chambers is that most designs require glue to seal the chamber[2–7]. To polymerize the glue and prevent outgassing within the high vacuum of the TEM, the entire environmental chamber with solution already present is either heated for several hours at ~70° C or exposed to intense ultraviolet irradiation [2, 7].

CORRESPONDING AUTHOR: Address: University of California at Davis, Department of Molecular and Cellular Biology, 1 Shields Avenue, Davis, CA 95616, JEEvans@UCDavis.edu, Phone: 1-530-752-8282, Fax: 1-520-752-3085.

SUPPORTING INFORMATION AVAILABLE: Experimental Procedures, Figures S1–S3, Movie S1 and corresponding Figure Legends are available free of charge via the Internet at http://pubs.acs.org.

Unfortunately, not all samples (biological proteins) or reactions (multi-component) are suited for such preparation and subsequent imaging conditions.

Here, we describe the implementation of a continuous flow *in situ* liquid stage that permits imaging complex multi-component reactions in real-time while extending the attainable spatial resolution to the atomic scale. We demonstrate control over the growth mechanisms that dictate the final morphology of nanostructures by varying the chemical composition and dilution of the reactant solution. We also show that an external laser can initiate nanoparticle growth independent of the imaging electrons allowing a wide range of physical, chemical and biological processes to now be studied. Since the continuous flow *in situ* liquid stage only requires partial isolation against the high vacuum on the inside of the TEM, the fluid inlet and outlet channels (Figure S1 in Supporting Information) are maintained at ambient pressure to the outside environment and allow the introduction of new solution or chemical components at any point during an experiment. This new functionality expands the repertoire of samples amenable to *in situ* liquid TEM observation from simple single-stage reactions to any type of complex reaction involving biological, mineral, or inorganic components in either aqueous or organic solvents.

To test the continuous flow *in situ* liquid stage for imaging fluid based reactions, we utilized a multi-component solution previously used for *ex situ* lead sulfide (PbS) nanoparticle growth [9]. The water based solution contained lead acetate, polyvinyl alcohol, isopropyl alcohol and thioacetamide. For this solution, the selective decomposition of thioacetamide by illumination with high-energy electrons [9] results in free sulfur being released into solution. Surrounding lead ions react with the free sulfur to nucleate and grow PbS nanoparticles while the polyvinyl alcohol acts as a stabilizing surfactant. We chose to characterize the performance of the *in situ* stage with a spherical aberration corrected scanning TEM (STEM) instead of conventional TEM as the STEM imaging mode allows the high-energy electron beam to be introduced to the solution in a controlled, shorter, and more localized manner than parallel illumination conventional TEM. STEM imaging also yields higher contrast than conventional TEM, since the image is mostly incoherent and the signal intensity in dark field imaging is correlated approximately to the atomic number squared [10].

As one expects from *ex situ* solution based growth of PbS, less local availability of reactant ions results in slower growth rates and smaller final nanoparticle size [1]. This trend was also observed with our *in situ* liquid STEM experiments as diluting the reactant solution in pure water (1,000 – 5,000 fold over the initial *ex situ* concentration) resulted in different forms of growth under the same electron beam conditions. A continually scanning STEM probe imaging the 1,000x dilution (Figure 1a) resulted in growth occurring via coalescence of nanoparticles to form a thin film in less than 5 seconds. At 2,500x dilution, uniform growth occurs more slowly, and the nanoparticles begin as discrete structures but quickly merge into an interconnected network (Figure 1b). At this dilution, nucleation and growth is also seen in areas not directly stimulated by the electron beam due to diffusion of ions. Finally, at 5,000x dilution (Figure 1c), nanoparticles are monodisperse and growth occurs at a rate suitable for real-time imaging. At this dilution, an individual area can be imaged for more than 60 seconds without the formation of a thin film and thus statistics for individual nanoparticles can be acquired. Upon further dilution, the availability of reactants becomes too low for continued growth and progress terminates after all reactants in a local area are utilized. However, due to the design of the continuous flow stage, initiating fluid flow can replenish the reactants and restart nanoparticle growth.

Coupling the *in situ* liquid stage with direct real-time imaging via electron microscopy, enables the direct observation of nucleation density, growth mechanism and resulting size

and shape of independent PbS nanoparticles under varying reaction conditions, thereby providing both individual and population averaged statistics. The real-time nucleation and growth of individual nanoparticles from a multi-component solution can be seen in Figure 2 and Movie S1 (Supporting Information). By assuming that growth occurs uniformly along all three faces, we can estimate an overall growth rate as volume increase per movie frame. Figure 2e represents a plot of nanoparticle size versus time for the 5 individual nanoparticles of the time series and clearly shows growth of nanoparticles via monomer attachment from solution (blue, green, purple and red lines) along with the movement of an individual nanoparticle out of the field of view (green line). Particle coalescence and Ostwald ripening mechanisms have also been detected in similar movies. The smallest nanoparticle nucleus visualized in these experiments was 0.8 nm in diameter (Figure S1 in Supporting Information) which is equivalent to previous experiments using static *in situ* liquid TEM to observe the reduction and growth of platinum nanoparticles through a similar fluid path thickness [7].

For the movies acquired with STEM in this paper, the time lapse from one frame to the next is approximately 403 ms. Due to this frame rate, it is possible that the smallest physically formed nuclei could form and grow before the subsequent frame is acquired. This is illustrated in the plot of Figure 2e, where the growth rate for the nanoparticle indicated by the blue line between frames 3 and 4 is nearly twice that of growth rates from any of the nanoparticles following nucleation. The blue line also depicts a nanoparticle with a final diameter twice the size of the other nanoparticles. This suggests that a second nucleus was formed nearby the blue nanoparticle between frames 3 and 4 and coalesced to form a single nanoparticle prior to acquisition of frame 4. Together, these real-time imaging results illustrate that the current experimental setup allows quantifying nuclei density, nuclei size, growth kinetics and final nanoparticle size. It should be noted that variations in the dwell time or current density of the electron probe will affect the apparent nanoparticle growth rate. Therefore, care must be taken to regulate the experimental setup to permit accurate interpretation and quantification of the observed results. However, while aberration corrected STEM can be used to track the growth of individual nanoparticles with real-time movies, to fully understand the mechanisms of nucleation and growth, advanced temporal resolution imaging will be required. Direct electron detectors are currently being developed to provide faster imaging systems with sub-millisecond frame-rates [11]. Additionally, future improvements to the environmental chamber such as using thinner electron transparent membranes less than 50 nm thick should extend the attainable resolution and contrast further by reducing the scattering cross-section of the background support that the electrons must transmit to image the liquid solution.

Similar to dilution, adjusting the relative ratio of chemical components within the solution changes the observed reaction. However, instead of changing the rate of the reaction as seen with dilution experiments, varying the chemical composition results in the growth of differently shaped and sized nanoparticles. We varied the ratio of lead to sulfur ions in solution at values of 2:1, 1:1, and 1:1.25 (lead acetate: thioacetamide) while keeping all other imaging conditions equivalent including electron probe dwell time and magnification. As can be seen in Figure 3, increasing the thioacetamide content relative to lead ions within the *in situ* stage resulted in a shift from individual nanoparticle growth to the evolution of cluster-like or flower-like shaped nanoparticles as a response to intense electron irradiation. At a ratio of 2:1 (Pb:S), the nanoparticles grow to 30 nm average diameter and if growth is not quenched, individual particles will coalesce into chain-like structures (Figure 3a). At a ratio of 1:1 (Pb:S), fewer nanoparticles grow in an equivalent field of view but remain monodisperse with a smaller average diameter of 20 nm (Figure 3b). Finally, at a ratio of 1:1.25 (Pb:S), the nanoparticles grow as individual clusters that have a central nanoparticle

with flower-like extensions (Figure 3c). A correlated growth series of a single nanoflower is shown in Figure S2 (Supporting Information).

Typically, the final morphology of nanoparticles is strongly governed by the energy supply and flux of reactants subsequent to the formation of nuclei [1]. Thermodynamic growth occurs when there is a sufficient supply of energy and a low density of reactants that often results in the formation of spherical structures via uniform growth of all crystal faces [1]. In contrast, the kinetic growth regime occurs under non-equilibrium conditions with a high density of reactants and typically results in preferential or directional growth along a crystal face [1]. Surprisingly, under specific reaction conditions, multiple types of PbS nanoparticles grow simultaneously when exposed to electron irradiation suggesting both mechanisms for growth are occurring. For the 1:1.25 (Pb:S) reaction, all observed growth occurs as flower-like nanoparticles (Figure 3f). However, during the 2:1 (Pb:S) reaction growth of spherical, hexagonal, and trigonal nanoparticles can be detected in the same field of view (Figure 3a, d, e & g). Post-mortem analysis confirmed that all nanoparticles observed during the *in situ* experiments, including those that coalesce during continued growth, were crystalline with lattice spacings matching those known for PbS nanoparticles (Figure S3 in Supporting Information). Interestingly, the *in situ* growth of multiple types of nanoparticles from a single solution differs from previously published experiments using *ex situ* electron irradiation of bulk solutions of the same chemical composition [9]. For the *ex situ* reactions, all the solutions of varying composition (equivalent to those analyzed *in situ*) resulted in homogenous populations of monodisperse spherical nanoparticles. Thus, the visualization of both kinetically- and thermodynamically-controlled growth of PbS nanoparticles within the *in situ* stage using electron irradiation suggests that the growth mechanisms exhibited within a localized reaction area differ from that of bulk solution. Future incorporation of electrochemical and thermal regulation within the environmental chamber may help fully correlate *in situ* and *ex situ* experiments using the same energy source.

Previous *in situ* liquid TEM publications have described resolution in terms of the smallest nanoparticle observed in the image [4, 7, 8, 12]. Here, we demonstrate the first direct atomic resolution imaging of nanoparticles grown from solution *in situ* by using aberration corrected STEM and a thin fluid path thickness between 50 – 100 nm. During growth experiments, most of the nanoparticles appear to nucleate and grow in solution and as a result are highly mobile which restricts high-resolution imaging. However, some nanoparticles become attached or nucleate on the surface of the silicon nitride membrane and remain stable permitting atomic resolution imaging. Figure 3g shows a spherical nanoparticle attached to the SiN membrane with a lattice spacing of 0.21 nm corresponding to the (220) plane for PbS. This indicates that future *in situ* liquid experiments requiring atomic resolution for reliable mechanistic interpretation will need to incorporate the use of templated surface growth or enhanced adsorption techniques to mitigate nanoparticle mobility.

In order to gain further control over observed reactions, we utilized a Dynamic TEM (DTEM) [13, 14] to optically trigger the reaction within the *in situ* stage using a Nd:YAG second harmonic sample drive laser and ultrafast pulsed imaging electrons. The intention was to test whether it was possible to initiate nanoparticle growth using an energy source separate from the imaging electron beam. As seen in Figure 4a–c, in the absence of the sample drive laser, PbS nanoparticles did not grow under bright field pulsed TEM imaging conditions for a 1:1,000x dilution of 1:1 ratio Pb:S reactants over a period of 15 minutes. However, upon stimulation of the same area with a single sample drive laser pulse (0.6μJ energy with 30 μm $1/e^2$ beam radius), nanoparticles nucleate within seconds and grow for several minutes (Figure 4d–f). This does not appear to be an effect of cumulative electron irradiation since equivalent movies using pulsed imaging lack evidence of nanoparticle

growth in the absence of sample drive laser stimulation over a timespan of 30 minutes and longer. Thus, the liquid experiments performed in the DTEM show that an external laser can initiate particle growth and decouple the observed nanoparticle growth from that caused by intense electron beam irradiation. Interestingly, the continued illumination of an area with the sample drive laser completely inhibits growth of nanoparticles and is likely due to the high-energy laser pulses ablating nuclei before continued growth can occur.

In conclusion, we have observed nanomaterial growth from multicomponent solutions in real-time and with atomic resolution by combining aberration corrected STEM imaging with a continuous flow *in situ* liquid stage. We demonstrated the controlled growth of PbS nanoparticles by adjusting the composition and dilution of the solution as well as utilizing two different irradiation sources. In the future, pump-probe imaging with an aberration corrected DTEM may allow atomic spatial resolution of both static and mobile nanoparticles by using ultrafast imaging electron pulses to mitigate the detrimental effects of Brownian motion during data acquisition. The improved temporal resolution of the DTEM could also provide new insights into both kinetic and thermodynamic nanomaterial nucleation and growth processes. Coupling such optimized microscope platforms with future advancements to the continuous flow *in situ* liquid stage, such as electrochemical and thermal regulation, should further extend the applicability of this approach to other research disciplines. Specifically, thermal regulation will be of central importance for the direct observation of protein dynamics and other processes at the interface of biology and nanotechnology.

Supplementary Material

Refer to Web version on PubMed Central for supplementary material.

Acknowledgments

We thank Melissa Santala, Bryan Reed and Thomas LaGrange for experimental assistance with Dynamic TEM. Aspects of this work relating to Dynamic TEM were performed under the auspices of the U.S. Department of Energy, Office of Basic Energy Sciences, Division of Materials Sciences and Engineering, under contract No. DE-AC52-07NA27344. J.E.E. and N.D.B. acknowledge NIH funding support from NIH grant number 5RC1GM91755.

References

1. Schmid, G. Nanoparticles: From Theory to Application. 2. Wiley-VCH; Weinheim: 2010. p. 522
2. Radisic A, Ross FM, Searson PC. J Phys Chem B. 2006; 110(15):7862–8. [PubMed: 16610883]
3. Williamson MJ, Tromp RM, Vereecken PM, Hull R, Ross FM. Nat Mater. 2003; 2(8):532–6. [PubMed: 12872162]
4. de Jonge N, Peckys DB, Kremers GJ, Piston DW. Proc Natl Acad Sci U S A. 2009; 106(7):2159–64. [PubMed: 19164524]
5. Dukes MJ, Peckys DB, de Jonge N. ACS Nano. 2010; 4(7):4110–6. [PubMed: 20550177]
6. Peckys DB, Veith GM, Joy DC, de Jonge N. PLoS One. 2009; 4(12):e8214. [PubMed: 20020038]
7. Zheng H, Smith RK, Jun YW, Kisielowski C, Dahmen U, Alivisatos AP. Science. 2009; 324(5932): 1309–12. [PubMed: 19498166]
8. Grogan JM, Bau HH. Journal of Microelectromechanical Systems. 2010; 19(4):885–894.
9. Wu M, Zhong H, Jiao Z, Li Z, Sun Y. Colloids and Surfaces A: Physicochemical and Engineering Aspects. 2008; 313–314:35–39.
10. James EM, Browning ND. Ultramicroscopy. 1999; 78:125–139.
11. Denes P, Bussat J-M, Lee Z, Radmillovic V. Nuclear Instruments and Methods in Physics Research A. 2007; 579:891–894.
12. de Jonge N, Poirier-Demers N, Demers H, Peckys DB, Drouin D. Ultramicroscopy. 2010; 110(9): 1114–1119. [PubMed: 20542380]

13. Kim JS, Lagrange T, Reed BW, Taheri ML, Armstrong MR, King WE, Browning ND, Campbell GH. Science. 2008; 321(5895):1472–5. [PubMed: 18787163]
14. LaGrange T, Campbell GH, Reed BW, Taheri M, Pesavento JB, Kim JS, Browning ND. Ultramicroscopy. 2008; 108(11):1441–9. [PubMed: 18783886]
15. Turyanska L, Elfurawi U, Li M, Fay MW, Thomas NR, Mann S, Blokland JH, Christianen PC, Patane A. Nanotechnology. 2009; 20(31):315604. [PubMed: 19597263]
16. Wang LP, Hong GY. Materials Research Bulletin. 2000; 35(5):695–701.
17. Egorov N, Eremin L, Usov V, Larionov A. High Energy Chemistry. 2007; 41(4):251–254.
18. Yao S, Han Y, Liu W, Zhang W, Wang H. Materials Chemistry and Physics. 2007; 101(2–3):247–250.

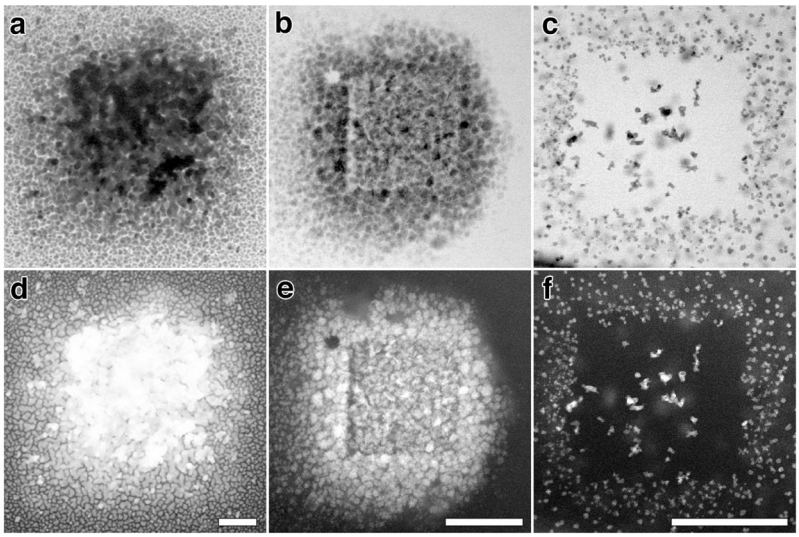

Figure 1. Overview images showing varying PbS growth mechanisms by changing effective dilution

Bright Field and Dark Field Scanning TEM overviews of the parent PbS solution diluted 1,000x (a & d), 2,500x (b & e) and 5,000x (c & f) centered on an area previously scanned at higher magnification. All panels depict evidence of ion diffusion causing nucleation and growth of nanoparticles in a region surrounding the square of initial electron irradiation. Scale bars represent 500 nm (d & e) and 250 nm (f).

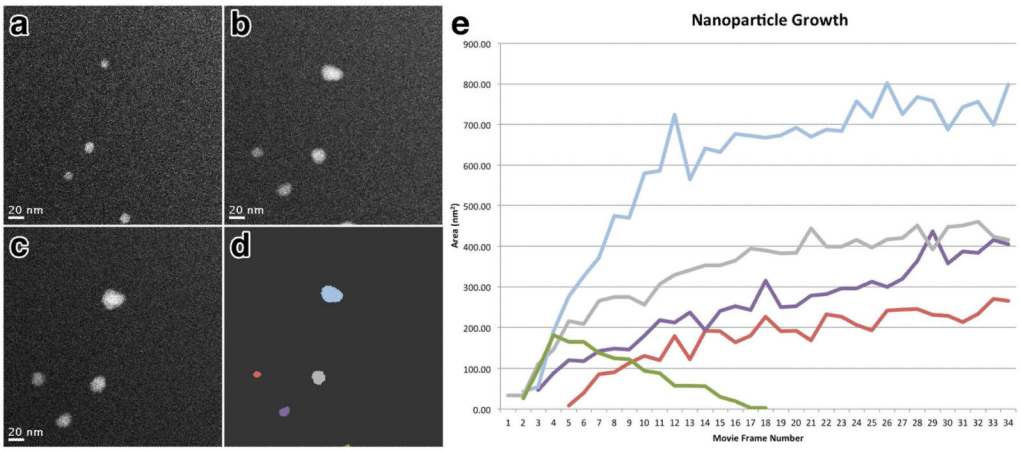

Figure 2. Tracking nanoparticle growth over time

Correlated image series of the same area at time = 3.5 seconds (a), 15.1 seconds (b) and 26.8 seconds (c) showing the growth of individual PbS nanoparticles. (d) depicts the same image as (b) with individual nanoparticles identified with varying color. (e) plot of nanoparticle area versus time spanning 40 seconds with lines representing individual nanoparticles labeled according to color as in (d). Panels (a–c) correspond to frames 3, 13 and 23 respectively. Scale bars represent 20 nm.

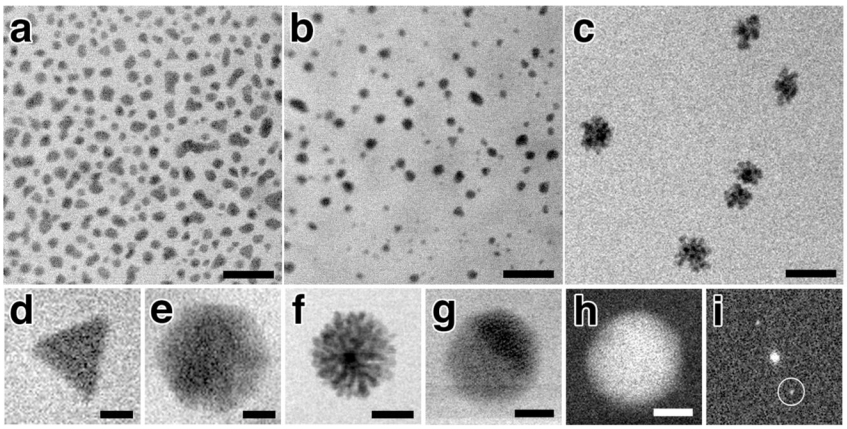

Figure 3. Nanoparticle growth under varying chemical composition of parent solution

In situ Bright Field Scanning TEM images of 2:1 (a), 1:1 (b) and 1:1.25 (c) Pb:S solutions each at 5,000x dilution. Panels (d–g) show a gallery of differently shaped nanoparticles observed *in situ* including trigonal (d), hexagonal (e) flower-like (f), and spherical (g). Dark Field Scanning TEM image (h) of the same nanoparticle in (g) and the corresponding FFT (i). Lattice fringes for the (220) plane of PbS at 0.21 nm resolution can be seen in (g&h) and Bragg reflections circled in (i). Scale bars represent 100 nm (a–c), 12.5 nm (d&e), 25 nm (f), and 2.5 nm (g&h).

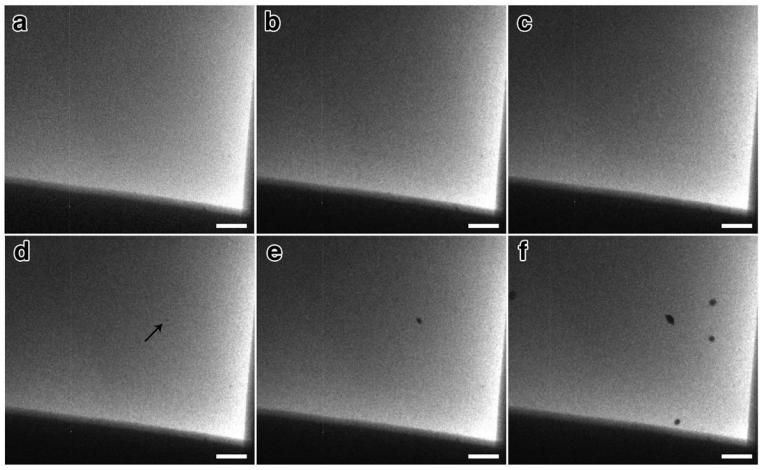

Figure 4. Controlled synthesis of nanoparticles using the Dynamic TEM sample drive laser

Correlated image series of the same area of a 1:1,000x dilution of 1:1 (Pb:S) solution illuminated solely with electron irradiation (a–c), or with electron irradiation but following a single sample drive laser pulse at an energy of 0.6 μj (d–f). For the electron irradiation only series, (a) corresponds to time = 0, while (b&c) are for time = 5 minutes and 15 minutes respectively. (d,e&f) correspond to the images 2 seconds, 2 minutes and 5 minutes after sample drive laser initiation, respectively. Arrow in (d) indicates first observed nuclei. Scale bars represent 3 μm.